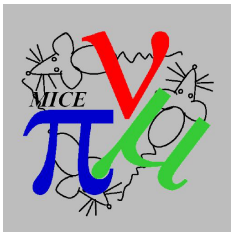

20th Century Fox

MICE-NOTE-499, November 2016

More Muon Cooling plus Emittance Exchange with a Wedge

Don Summers, Lucien Cremaldi, and David Sanders, University of Mississippi

Tanaz Mohayai and Pavel Snopok, IIT-Chicago

David Neuffer, Fermilab

Abstract

A longer absorber raises dE/dx loss and increases muon cooling linearly in the limit that the approach to equilibrium emittance is small. More cooling is easier to measure and reduces risk. A wedge can produce a large amount of emittance exchange. Emittance exchange is crucial for three purposes: 1) to store transverse cooling as a decrease in longitudinal beam emittance; 2) to prepare a flat muon beam for low β^* quadrupoles to decrease transverse emittance from 280 microns (achieved in simulation with short solenoids [1]) to 100 microns and complete 6D cooling [2]; 3) for reverse emittance exchange to decrease transverse emittance from 100 to 25 microns at the expense of longitudinal emittance for a high energy lepton collider [3].

1 Introduction

The international Muon Ionization Cooling Experiment, MICE [4], is designed to measure muon ionization cooling [1, 2, 5]. Cooling is needed for Neutrino Factories based on muon decay ($\mu^- \to e^- \overline{\nu}_e \nu_\mu$ and $\mu^+ \to e^+ \nu_e \overline{\nu}_\mu$) in storage rings [6] and for muon colliders [7]. A variant of muon cooling is also being used in Japan to measure g-2 [8].

We explore longer absorber lengths in Section 2 and note that an experiment with more energy loss and therefore more first order cooling could fit within the MICE configuration. In following sections, we consider the use of wedge absorbers to extend the MICE cooling explorations, but we have left the wedge absorbers with the same average energy loss as the initial MICE Step 4 baseline absorbers.

2 More Cooling with a Longer Absorber

The current lithium hydride absorber at MICE is 65 mm thick and 45 cm in diameter. For a 200 MeV/c muon beam with a kinetic energy of 121 MeV this provides an 11.3 MeV energy loss, which is 9% of the beam kinetic energy. Two additional 32 mm by 45 cm diameter lithium hydride disks may be coming. These would raise the fractional energy loss to 18%. Cooling increases with fractional energy loss as noted in equation 1.

$$\frac{d\epsilon_\perp}{ds} = -\frac{g_t}{\beta^2}\frac{dE_\mu}{ds}\frac{\epsilon_\perp}{E_\mu} + \frac{1}{\beta^3}\frac{\beta^*_\perp}{2}\frac{(13.6\,\mathrm{MeV})^2}{E_\mu m_\mu c^2 L_R} \tag{1}$$

Table 1: Muon equilibrium emittance at 200 MeV/c (β = v/c = 0.88, KE = 121 MeV) for hydrogen, deuterium, lithium hydride, lithium, beryllium, boron carbide, polyethylene, diamond, and beryllium oxide absorbers [9, 10].

Material	Density	L_R	dE/ds	$L_R \times$ dE/ds	$\epsilon_\perp$ (mm equilibrium)	
	g/cm^3	cm	MeV/cm	MeV	$\beta^* = 1$ cm	$\beta^* = 50$ cm
H_2 gas	0.000084	750,000	0.00037	278	0.036	1.80
H_2 liquid	0.0708	890	0.313	278	0.036	1.80
D_2 liquid	0.1638	769	0.362	278	0.036	1.80
^{6}Li H	0.72	∼97	∼1.73	168	0.059	2.95
Li H	0.82	97	1.73	168	0.059	2.95
Li	0.53	155	0.96	149	0.067	3.35
Be	1.85	35.3	3.24	114	0.087	4.35
CH_2	0.89	50.3	2.05	103	0.096	4.80
B_4C	2.52	19.9	4.57	90.9	0.109	5.45
Diamond	3.52	12.1	6.70	81.1	0.123	6.15
Be O	3.01	13.7	5.51	75.5	0.132	6.60

The liquid hydrogen absorber is 350 mm long [11] providing an energy loss of 11.0 MeV. The same 350 mm length of lithium would provide a 33.6 MeV energy loss. Lithium may be stored under argon, mineral oil, or a layer of paraffin wax to keep it away from water, oxygen, and nitrogen [12]. Multiple scattering in lithium has been measured in a muon beam at TRIUMF [13].

A 200 mm length of polyethylene would provide an energy loss 41.0 MeV, twice the loss of 130 mm of LiH. If the muon kinetic energy fell from 140 to 100 MeV, the muon momentum would fall from 222 to 177 MeV/c. The upstream and downstream spectrometer magnetic elements would need to be tuned to 222 and 177 MeV/c, respectively. The polyethylene equilibrium emittance, as noted in Table 1, is 4.8 mm for a β^* of 50 cm. So an initial beam emittance of 12 mm may be a good match, if this large an emittance can be achieved. Note that the beta function, $\beta(s)$, is determined exclusively by the magnetic lattice, $K(s)$, which is a function of magnetic fields and the muon momentum. Solving equation 2 [14] in a field region where K(s) = 0, one finds that β^* increases quadratically from a minimum at s = 0 as noted in equation 3 [15]. The absorber length is limited to be perhaps as large as β^*. Finally, a β^* as low as 50 cm may be possible at MICE [16], even in the absence of the downstream spectrometer M1 matching coil.

Table 2: Polyethylene wedge simulations run at 200 MeV/c. The equilibrium emittance for polyethylene, given a β^* of 50 cm, is 4.8 mm.

Angle	Center to Apex	Beam Center	Reverse Emittance Exchange	Energy Cooling
degrees	cm	Thickness	$\eta = 0$	$\eta = 0.3$ m
		cm	$\sigma_p = 2$ MeV/c	$\sigma_p = 10$ MeV/c
60	5	5.77	4.0	
30	10	5.36	2.1	20%
0	NA	5.4		

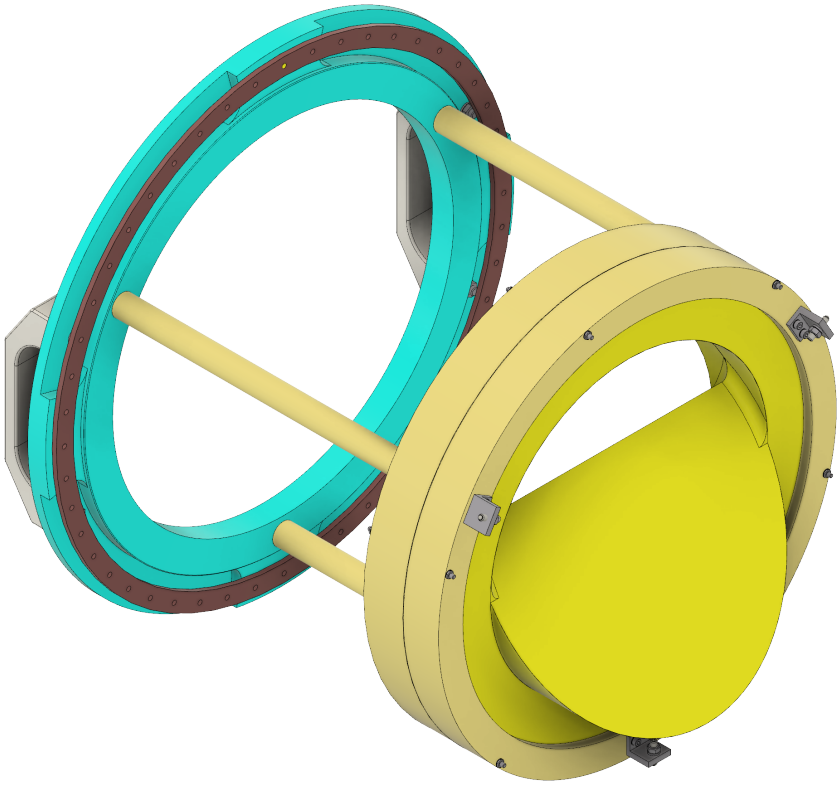

Figure 1: 60° polyethylene wedge

In Table 1, $\epsilon_\perp = \beta^* E_s^2/(2 g_x \beta\, m_\mu c^2 (dE/ds) L_R)$, where β^* is the Courant Snyder parameter, E_s is 13.6 MeV, the transverse damping partition number g_x is one with parallel absorber faces, $m_\mu c^2$ is 105.7 MeV, and L_R is radiation length. Note that 92.4% of natural lithium has seven nucleons and 7.6% has six nucleons. The lithium in Oak Ridge lithium hydride has six nucleons. The densities for ^{6}Li, natural Li, and ^{7}Li are 0.460, 0.531, and 0.537 g/cm^3, respectively [17].

$$\frac{1}{2}\beta\beta'' - \frac{1}{4}\beta'^2 + \beta^2 K(s) = 1 \tag{2}$$

$$\beta(s) = \beta^*[1 + ((s - s_0)/\beta^*)^2] \tag{3}$$

3 Wedges and Emittance Exchange

Polyethylene wedge absorbers with 60^0, 30^0, and 0^0 (flat) might be used at MICE (see Fig. 1). A 30^0 wedge with a 50 cm dispersion and 5% dp/p (sigma) gives a ∼20% longitudinal emittance decrease, as noted in Table 2. MICE can thus measure 6D cooling. Emittance exchange for transverse emittance decrease or longitudinal emittance decrease can be obtained with an initial emittance of 3 mm [9]. In reverse emittance exchange with a 60^0 wedge, the x transverse emittance goes down by a factor of four, while the longitudinal emittance goes up by a factor of four. And if the initial beam emittance is 12 mm, polyethylene should cool. This will decrease in the wedge direction by the partition number g_t. Note that dispersion comes from picking the right ensemble of muons

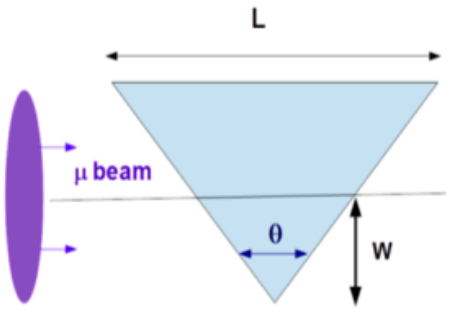

Figure 2: Schematic view of a muon beam passing through a wedge.

rather than from an actual dipole. The dispersion should be less than β^* to prevent additional beam heating from a coupling of multiple scattering and longitudinal straggling [9, 18].

A fair amount MICE wedge design work has already been done [19]. Plates of UHMW polyethylene are available from McMaster Carr, including 24" x 24" x 5" pieces.

4 Simulations of Beams in Wedge Configurations

We have done a number of initial simulations of beam passing through possible wedges. These initial simulations were performed in ICOOL [20], and assumed idealized beams inserted just before the wedge and tracked into just after the wedge.

In the present note we track beam through polyethylene wedges (C_2H_4) at parameters similar to those that can exist in the MICE beam. As a reference MICE beam we consider a 200 MeV/c Gaussian μ beam with $\epsilon_{t,N} = \sim 0.003\,\mathrm{m}$ and momentum spreads chosen to be matched to the requirements of emittance exchange scenarios.

Polyethylene (Poly) is chosen because it is inexpensive, readily available and can be easily machined into the desired shapes. It is a relatively low-Z material (C and H) with relatively little multiple scattering. Lower Z materials (Li, H, LiH, Be) would be a bit better for cooling but are more difficult to obtain, machine, and insert within the present limitations of the MICE experiment. Poly wedges could adequately demonstrate and explore the basic emittance exchange processes needed in future μ accelerators. Following previous studies, Poly has a density of 0.94 gm/cm^3, radiation length $X_0 = 47.5$ cm, mean ionization energy of $I = 57.43$ eV, implying energy

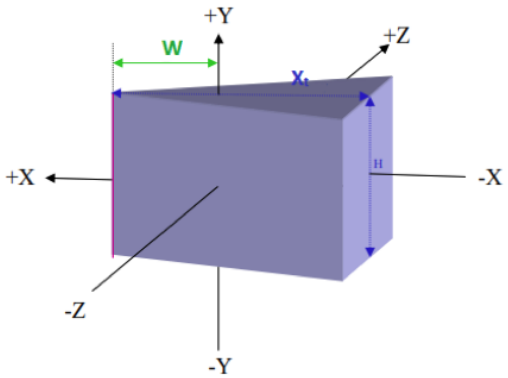

Figure 3: Another view of the wedge geometry. Beam is directed along the z axis.

Table 3: Beam parameters at entrance, center, and exit of a $w = 5$ cm, $\theta = 60^\circ$ C_2H_4 wedge.

z (cm)	p_z (MeV/c)	σ_E (MeV)	ϵ_x (mm)	ϵ_y (mm)	ϵ_z (mm)
0	200	1.8	3.0	3.0	2.9
6	193	3.9	1.44	3.0	6.8
12	182	8.6	0.76	3.0	14.3

loss of $\sim$2.17 MeV/cm at 200 MeV/c. 5 cm provides $\sim$11 MeV of energy loss, similar to other absorbers used as MICE coolers.

Three wedges are considered in the present exploration, based on wedge angles of 60°, 30°, 0°, with the central width near 5 cm. Figs. 2 and 3 show a schematic view of μ beam passing through a wedge, and Table 2 shows parameters of the wedge examples. The 60° case can simulate the large transverse/longitudinal emittance exchange needed in final cooling scenarios. The 30° wedge can demonstrate longitudinal/transverse exchange in configurations where either the longitudinal or transverse emittance is reduced. The 0° case provides a comparison flat absorber with about the same average width as the wedges.

4.1 Simulation Results

We first consider the 60° case. The beam entering the wedge is matched to $\sigma_x = 2.5$ cm, ($\epsilon_t = 3$ mm, $\beta_t = 36$ cm) with $p_0 = 200$ MeV/c, corresponding to a baseline MICE beam setting, but with $\delta p = 2$ MeV/c. This example obtains an increase in δp by a factor of $\sim$4 accompanied by a reduction in ϵ_x by a factor of $\sim$4 in ICOOL simulation. Results are displayed in Table 3 and displayed in Figs. 4 and 5.

The MICE μ beam naturally has a momentum spread much larger than this ($\sigma_{\delta p} \sim$10-20 MeV/c). The small δp is obtained by software selection of a $\sigma_{\delta p} = 2$ MeV/c sample from the incident beam, which consists of individually measured muons.

Because the 60° absorber is matched to $\sim 2\sigma$ for the above reference MICE beam, it cannot accept a significantly larger beam, and cannot explore significantly different configurations.

With the 30° absorber, we can explore larger beams including those with larger δp and dispersion, which can be cooled longitudinally, as well as transverse emittance reduction (with small initial δp, similar to the 60° wedge above, but with less exchange). We consider two complementary

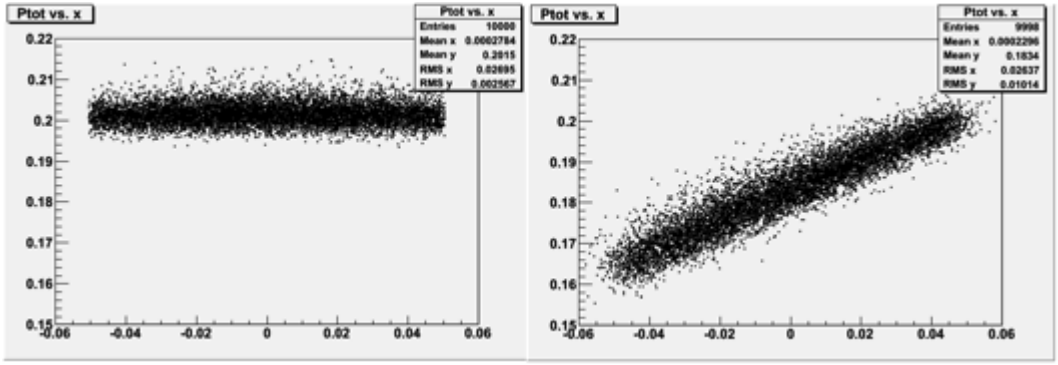

Figure 4: x-p projection of beam before and after the MICE wedge.

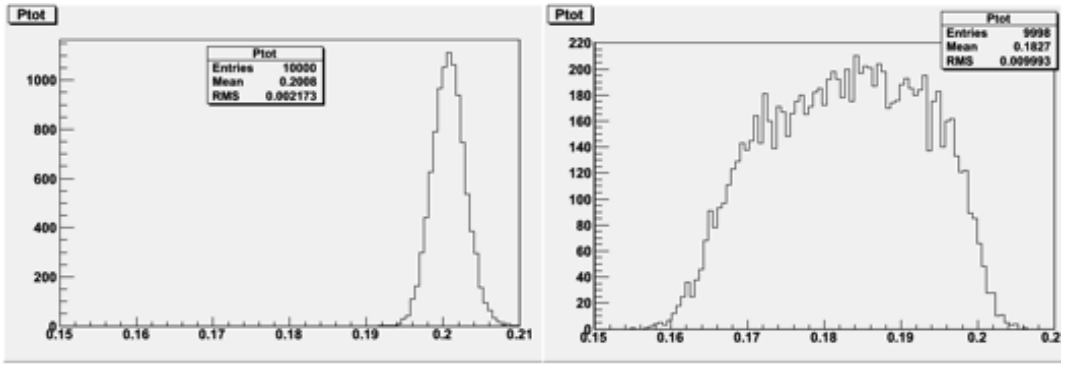

Figure 5: Momentum spread distributions before and after the 60° polyethylene wedge. (Assumes a $\sigma_{\delta p} = 2$ MeV/c initial distribution with $\sigma_x = 2.5$ cm.)

examples: Case I: a beam with small δp similar to that used for the 60° wedge, and II: a similar transverse emittance beam but with a $\sim$0.5 m initial dispersion oriented to reduce δp and therefore longitudinal emittance.

The MICE beam has no intrinsic dispersion and a dispersive beam would have to be generated by software selection of initial beam tracks, much like the small δp beam.

ICOOL simulations of these simple cases are presented in Table 4. In the Case I, emittance exchange is similar to the above 60° example, but the exchange is reduced to a factor of 2.25, following the decrease in angle from 60 to 30. In Case II, the longitudinal emittance is reduced by $\sim$20% while the horizontal emittance increases by a factor of $\sim$30%. Note that at the parameters presented the dispersion is matched to nearly zero after the wedge, which may facilitate analysis by decoupling the transverse and longitudinal motion downstream of the absorber.

With the 0° absorber, no wedge-specific effects occur, and only energy-loss transverse cooling can occur. However, at expected MICE beam parameters ($\beta_t = 0.5$ m) the equilibrium emittance is $\sim$5mm with Poly absorbers. With the $\sim$3 mm beams presented above, the beam is heated by the absorber. In order to obtain cooling the initial emittance must be significantly greater than that. The experiment would be useful for comparison with wedge absorber results, isolating wedge effects from solid absorbers.

Table 5 shows results of ICOOL simulations with the 0° absorber. Beam is heated with the 3 mm initial emittance, and only slightly cooled at 6 mm.

Table 4: Beam parameters at entrance and exit of a $w = 10$ cm, $\theta = 30°$ C_2H_4 wedge.

	p_z MeV/c	ϵ_x mm	ϵ_y mm	ϵ_z mm	δE MeV rms	η m	β_t m
Case I before	200	3.06	2.97	2.92	1.82	0.0	0.5
Case I after	183.3	1.36	2.65	8.18	4.76	1.14	0.43
Case II before	200	2.95	3.03	14.5	8.82	0.51	0.45
Case II after	183.3	3.82	3.09	12.3	7.60	0.02	0.49

Table 5: Beam parameters at entrance and exit of a $L = 5.4$ cm, $\theta = 0°$ C_2H_4 wedge.

	p_z	ϵ_x	ϵ_y	ϵ_z	δE	η	β_t
	MeV/c	mm	mm	mm	MeV rms	m	m
Case I before	200	3.12	3.04	14.3	8.82	0.0	0.45
Case I after	186.5	3.20	3.11	14.7	9.07	0.0	0.45
Case II before	200	6.17	6.00	14.4	8.83	0.0	0.504
Case II after	186.5	6.09	5.92	14.8	9.08	0.0	0.515

4.2 Discussion

The simulations presented here are based on idealized uncoupled beam passing through the absorbers, without restricting apertures. In the MICE experiment, solenoidal focusing couples the beam, and x and y emittances are less clearly separated. Some care in emittance reconstruction is required.

The MICE experiment has lately been somewhat limited in focussing capability by the loss of a downstream coupling coil and the consequent conservative limits on magnet operation. The acceptance of the cooling channel is reduced, and beam optics matching is more limited. Obtaining the smaller β^* values at the absorber may be difficult. Emittances $> \sim 6$ mm may not be useable.

Parameters of an operating experiment may need to be modified from the simplified examples presented here. Simulations of the full cooling channel with the existing magnet limitations are needed. We are confident that a significant exploration of the role of wedge absorbers in ionization cooling will be possible.

References

[1] D. Stratakis and R. B. Palmer, Phys. Rev. ST Accel. Beams **18** (2015) 031003;
D. Stratakis *et al.,* Phys. Rev. ST Accel. Beams **16** (2013) 091001.

[2] J. G. Acosta *et al.,* COOL-2015-MOPF07;
J. G. Acosta *et al.,* SESAPS-2015-C203;
J. G. Acosta, Ph.D. Dissertation, 2016;
T. L. Hart *et al.,* NAPAC-2016-TUPOB44;
D. Summers *et al.,* IPAC-2015-TUPWI044;
D. Summers *et al.,* FERMILAB-TM-2603-AD-APC;
Al Garren and Harold Kirk, MAP-DOC-4408 (2002);
H. Kirk *et al.,* Conf.Proc. **C030512** (2003) 2008;
A. Garren *et al.,* AIP Conf. Proc. **821** (2006) 432;
S. Oliveros *et al.,* SESAPS-2015-F1-4;
J. Acosta *et al.,* SESAPS-2015-C2-3;
M. M. Alsharo'a *et al.,* Phys. Rev. ST Accel. Beams **6** (2003) 081001.

[3] D. Neuffer, AIP Conf. Proc. **441** (1998) 270;
D. Neuffer *et al.,* IPAC-2016-THPOR025.

[4] M. Bogomilov *et al.,* JINST **7** (2012) P05009;
D. Adams *et al.,* Eur. Phys. J. **C73** (2013) 2582;

D. Adams *et al.,* JINST **10** (2015) P12012 ;
L. Cremaldi *et al.,* IEEE Trans. Nucl. Sci. **56** (2009) 1475;
R. Bertoni *et al.,* Nucl. Instrum. Meth. **A615** (2010) 14;
M. Ellis *et al.,* Nucl. Instrum. Meth. **A659** (2011) 136;
M. Bogomilov *et al.,* JINST **11** (2016) P03001;
M. Bogomilov *et al.,* "Scattering of 240 MeV/c Muons with Gaseous Xenon in MICE" (2016);
MICE, "Design and expected performance of the MICE Demonstration of Ionization Cooling;"
K. Long, Nucl. Part. Phys. Proc. **273 -275** (2016) 162;
D. M. Kaplan *et al.,* NuFact15, arXiv:1601.07202;
T. Luo and D. Li, IPAC -2016 -MOPMW029;
Y. Torun *et al.,* IPAC -2016 -MOPMW034;
R. Asfandiyarov *et al.,* arXiv:1607.04955;
Ao Liu, NAPAC -2016 - MOA2CO04;
A. Dobbs *et al.,* arXiv:1610.05161.

[5] A. N. Skrinsky and V. V. Parkhomchuk, Sov. J. Part. Nucl. **12** (1981) 223;
D. Neuffer, Part. Accel. **14** (1983) 75;
J. Norem *et al.,* Phys. Rev. ST Accel. Beams **6** (2003) 072001;
A. Moretti *et al.,* Phys. Rev. ST Accel. Beams **8** (2005) 072001;
A. Hassanein *et al.,* Phys. Rev. ST Accel. Beams **9** (2006) 062001;
P. M. Hanlet *et al.,* EPAC06-TUPCH147;
R. B. Palmer *et al.,* Phys. Rev. ST Accel Beams **8** (2005) 061003;
P. Snopok *et al.,* Int. J. Mod. Phys. **A24** (2009) 987;
J. C. Gallardo and M. S. Zisman, AIP Conf Proc. **1222** (2010) 308;
M. Chung *et al.,* Phys. Rev. Lett. **111** (2013) 184802;
C. Yoshikawa *et al.,* IPAC -2014 -TUPME016;
D. Stratakis *et al.,* Phys. Rev. ST Accel. Beams **18** (2015) 044201;
Y. Bao *et al.,* Phys. Rev. Accel. Beams **19** (2016) 031001;
B. Freemire *et al.,* Phys. Rev. Accel. Beams **19** (2016) 062004.

[6] D. G. Koshkarev, CERN-ISR-DI-74-62 (1974);
D. Neuffer, Telemark Lodge, Wisconsin, TELE -1980 - 040;
D. Cline and D. Neuffer, AIP Conf. Proc. **68** (1980) 856;
D. Neuffer, IEEE Trans. Nucl. Sci. **28** (1981) 2034;
S. Ozaki, R. B. Palmer, M. S. Zisman *et al.,* BNL -52623 (2001);
S. Choubey *et al.,* arXiv:1112.2853;
D. Adey *et al.,* arXiv:1308.6822;
D. Adey *et al.,* Phys. Rev. **D80** (2014) 071301.

[7] G. I. Budker, Conf. Proc. **C690827** (1969) 33;
A. N. Skrinsky, Morges, AIP Conf. Proc. **352** (1996) 6;
D. Neuffer, FERMILAB -FN - 0319 (1979);
D. Neuffer, AIP Conf. Proc. **156** (1987) 201;
D. Neuffer and R. Palmer, Conf.Proc. C940627 (1995) 52;
D. B. Cline, AIP Conf. Proc. **352** (1996) 19;
R. B. Palmer *et al.;* AIP Conf. Proc. **352** (1996) 108;
R. B. Palmer *et al.,* AIP Conf. Proc. **372** (1996) 3;
R. B. Palmer *et al.,* Nucl. Phys. Proc. Suppl. **51A** (1996) 61;
J. C. Gallardo *et al.,* Snowmass 1996, BNL - 52503;

R. Raja and A. Tollestrup, Phys. Rev. **D58** (1998) 013005;
C. M. Ankenbrandt *et al.,* Phys. Rev. ST Accel. Beams **2** (1999) 081001;
D. J. Summers *et al.,* PAC07-THPMS082;
D. J. Summers *et al.,* IPAC-2012-THPPD020;
G. T. Lyons III, Master's thesis, arXiv:1112.1105;
Y. Alexahin *et al.,* Phys. Rev. ST Accel. Beams **14** (2011) 061001;
M. A. Cummings, arXiv:1511.01423;
D. Neuffer *et al.,* NAPAC-2016-TUPOB06.

[8] Tsutomu Mibe, "Measurement of muon g-2 and EDM with an ultra-cold muon beam at J-PARC," Nucl. Phys. Proc. Suppl. **218** (2011) 242;
M. Otani *et al.,* Phys. Rev. Accel. Beams **19** (2016) 040101;
M. Otani *et al.,* IPAC-2016-TUPMY003.

[9] D. Neuffer, arXiv:1312.1266.

[10] K. A. Olive *et al.,* Chin. Phys. **C38** (2014) 090001;
http://pdg.lbl.gov/2014/AtomicNuclearProperties/

[11] M. A. C. Cummings, PAC-2005-WPAE022;
M. A. Cummings, Int. J. Mod. Phys. **A20** (2005) 3847.

[12] https://web.stanford.edu/dept/EHS/prod/researchlab/lab/safety_sheets/15-075.pdf.

[13] D. Attwood *et al.,* Nucl. Instrum. Meth. **B251** (2006) 41.

[14] E. D. Courant and H. S. Snyder, Annals Phys. **3** (1958) 1, equation 3.28.

[15] M. Sands, SLAC-R-121 (1970), equation 2.81.

[16] A. Liu, "MICE Step IV Optics without the M1 Coil in SSD," IPAC-2016-TUPMY006.

[17] D. D. Snyder and D. J. Montgomery, "Bulk Density of Separated Lithium Isotopes," J. Chem Phys. **27** (1957) 1033.

[18] C. X. Wang and K. J. Kim, Nucl.Instrum. Meth. **A503** (2003) 401;
C. X. Wang and K. J. Kim., Nucl. Instrum. Meth. **A532** (2004) 260.

[19] C. T. Rogers, P. Snopok, L. Coney, and A. Jansson, "Wedge Absorber Design for the Muon Ionisation Cooling Experiment," MICE-NOTE-290 (2010);
C. T. Rogers, P. Snopok, L. Coney, and G. Hanson, "Wedge absorber design and simulation for MICE Step IV," PAC-2011-MOP060;
D. Neuffer, T. Mohayai, P. Snopok, J. Acosta, and D. Summers, NAPAC-2016-WEPOA35.

[20] R. C. Fernow, PAC-1999, BNL-66248;
R. C. Fernow, PAC-2005-TPPP041.